Materials and Design 50 (2013) 1011–1018

Contents lists available at SciVerse ScienceDirect

Materials and Design

journal homepage: www.elsevier.com/locate/matdes

Experimental and numerical analysis of thermal shock damages to alumina based ceramic disk samples

Marija M. Dimitrijević *, Bojan Medjo, Radmila Jančić Heinemann, Marko Rakin, Tatjana Volkov-Husović

University of Belgrade, Faculty of Technology and Metallurgy, Karnegijeva 4, Belgrade, Serbia

ARTICLE INFO

Article history:
Received 19 December 2012
Accepted 29 March 2013
Available online 11 April 2013

Keywords:
Alumina ceramics
Finite element method
Image analysis
Thermal shock

ABSTRACT

Thermal shock of an alumina-based ceramic material, which occurs widely in metallurgical furnaces, was studied in this paper. The water quench test was applied to determine the thermal shock resistance of the material. The behavior of the ceramics after thermal shock treatments was investigated. The level of degradation of the samples was monitored using image analysis tools and the defects morphology characteristics were simultaneously determined. The stress state of the samples with simplified damage shapes was simulated by the finite element method (FEM) and the influence of the surface damage geometry on the stress in the sample was examined. The analysis revealed that the surface defects tend to spread on the surface of the specimen instead of increasing their depth. This explained the morphology of defects and the way of propagation of the damage that were in accordance with experimental observations.

1. Introduction

Alumina-based ceramics are used in many special applications where density, high hardness, chemical inertness and good high temperature properties are required. Alumina ceramics are known for high hardness and good resistance to oxidation, thermal shock, and corrosion. These excellent thermo-mechanical properties of alumina materials, as compared to those of conventional metals, suggested the employment of alumina in high-temperature environments [1].

The thermal stability of refractory materials is defined as the resistance of the material to sudden temperature changes. Refractory materials are built into the walls of furnaces and aggregates that are exposed to the influence of heat waves of greater or less intensity. For certain parts of the industrial furnaces, where the thermal gradients are especially important, the necessity for the use of materials with high thermal stability is paramount. Thermal stability could be viewed from two perspectives: the heat transfer and/or fracture mechanics [2].

Refractory material develops induced stress when exposed to sudden temperature changes [3]. Unequal expansion occurs for three possible reasons: a nonlinear temperature profile along the body, material inhomogeneity and the anisotropic nature of the material.

The classic theory on the thermal shock resistance of brittle ceramics was established by Hasselman [4,5]. Yuan et al. [6] investigated the correlation between the porosity of ceramics and their resistance to thermal shock. The main attention was directed to crack growth, and it was found that the extent of cracking that occurred during the quenching of a heated body into water at room temperature depended on the value of the temperature change, ΔT, and the volume fraction of pores. At lower temperatures differences, relatively few cracks were formed, but at the highest values of ΔT there was a tendency for the occurrence of lateral growth of cracks and some cracks had a "fir-tree" structure. Thermal shock resistance of Al_2O_3–TiC composites was compared with varying particle sizes of Al_2O_3 with monolith by You et al. [7]. The addition of TiC particles to the alumina matrix decreased the Al_2O_3 grain size, improved the mechanical properties and thermal shock resistance of the composites. Thermal quenching of refractories leads to a nucleation and/or crack propagation, resulting in loss of strength [8].

Stress at any point is determined by the temperature distribution in the sample, the sample shape and the physical properties such as: Young's modulus, coefficient of thermal expansion, heat capacity, heat conductivity and the Poisson ratio. When all these parameters are known, the strain can be calculated at any point of the body [9].

In a thermal shock experiment, when the change in the temperature exceeds the critical temperature difference of the material, the tensile stress generated in the material, due to the temperature gradient, exceeds the actual tensile strength of the material, resulting in failure of the material. There are many test methods available to characterize thermal shock of ceramic materials. Many

* Corresponding author. Tel.: +381 113303616; fax: +381 113370387.
E-mail addresses: mdimitrijevic@tmf.bg.ac.rs (M.M. Dimitrijević), bmedjo@tmf.bg.ac.rs (B. Medjo), radica@tmf.bg.ac.rs (R. Jančić Heinemann), marko@tmf.bg.ac.rs (M. Rakin), tatjana@tmf.bg.ac.rs (T. Volkov-Husović).

0261-3069/$ - see front matter © 2013 Elsevier Ltd. All rights reserved.
http://dx.doi.org/10.1016/j.matdes.2013.03.100

authors extensively studied thermal shock of alumina by considering various parameters, e.g., temperature, thermal stress distribution and effect of critical grain size on thermal shock. Thermal shock of ceramics yields thermal stress, which is, in some cases, sufficient to cause considerable cracking damage. Destruction of the samples was further analyzed using image analysis tools. This is a very convenient method for determining the level of surface damage of a sample resulting from thermal shock [10].

The use of mathematical modeling for descriptions of the temperature field and the corresponding stress field is based on the use of the finite element method (FEM) for simulation of these parameters. The effect of the maximum stressed region (crack initiation zone) of a sample after thermal shock was simulated in [11] using FEM software to obtain thermal stress distributions.

Panda [12] studied thermal shock and the thermal fatigue behavior of alumina. The thermal stress values resulted from the modeling of alumina samples of different thickness. The critical temperature difference depended on the thickness of the sample and was higher for thicker samples. This was because a higher temperature was necessary to develop the same stress level in a thicker sample. Thermal fatigue tests were conducted by indenting near the periphery of the heating surface that would experience the maximum thermal stress during heating. The number of thermal fatigue cycles decreased with increasing temperature difference of the cycles. Li et al. [13] performed numerical simulation with a 2D geometry using the finite element method to model microcrack growth during thermal shock. A comparison of experimental results with numerical results showed that after 25 thermal shock cycles, the crack growth in simulation result agreed well with the corresponding experimental result. Many experimental, analytical and numerical studies of thermal shock damage in brittle materials could be found in the literature. Thermal shock resistance is one of the most important parameters in the characterization of ultra high temperature ceramics. To analyze the effect of thickness of the sample on thermal stress, the finite element method was used for simulation of the temperature and thermal stress distribution during thermal shock tests. Hongbing et al. calculated the thermal stresses in a SiC–Al_2O_3 composite tritium penetration barrier on 316L stainless steel [14]. The stress discontinuity at the interface and the residual stresses at the interface were analyzed taking into account the graded properties of the coating. Further studies of high temperature insulation ceramic coatings were also conducted using the same method [15] for the determination of the dependence of the residual stress on the coating thickness. A simulation of the thermal shock induced damage in borosilicate glass was presented in [16]. The elastic properties of the glass and the effect of damage due to thermal shock on the residual stiffness of the glass were determined by vibration tests. The influence of the surface finish of alumina samples on thermal shock behavior was analyzed by numerical simulation in [17], in which three different FE models (with different levels of simplification) were considered. Thermal shock behavior of functionally graded materials (planar alumina/zirconia FGM) was studied in [18]. The results of the thermal shock tests (studied by the indentation-quench technique) were compared to those of homogenous alumina, showing a highly enhanced resistance of the FGM against transversal propagation of surface cracks. Thermal shock of a composite material with the same constituents (alumina and zirconia) was analyzed using the mesh-free method in [19]. Fracture mechanics analysis of alumina exposed to sudden cooling was conducted using the FEM in [20], using a two dimensional model for the determination of the factors influencing the induced stress intensity.

Destruction of the samples was analyzed using image analysis tools in this work. This is a very convenient method for determining the level of surface damage of a sample induced by thermal shock. The effect of the maximum stressed region (damage with simplified geometry) on the thermal shock is simulated using the finite element method (FEM) to obtain the thermal stress distributions experienced by the specimens.

The aim of this paper was to examine the locations of stress concentration during thermal shock and the residual stress in the material after heating and cooling the sample. In addition, the dependence of the obtained stress on the shape and geometry of the damage was assessed. These analyses were conducted by the finite element method, using the software package Abaqus [21].

2. Experimental details

2.1. Material

The starting materials used to create the samples, chamotte, bauxite and clay, were the same as the ones used for industrial production in Samot Arandjelovac. The components were milled with Al_2O_3 balls in deionized water in a polyethylene bottle. The samples were then pressed into cylinders of dimensions 30×9 mm at a pressure of 36 MPa or 50 MPa. The pressed samples were sintered at 1200 °C for 2 h in an oxidative atmosphere.

The mass fractions of the raw materials used are given in Table 1. The structure of the obtained material was examined by the X-ray diffraction, XRD, technique and the obtained result is given in Fig. 1.

2.2. Thermal shock

The thermal stability of the refractories was determined experimentally by the water quench test [22]. The sample was heated in an electric furnace at a temperature of 950 °C for 40 min and then quenched in water to a depth of 50 mm, where the temperature was between 20 and 25 °C. The sample was kept in the water for about 3 min, removed and dried in air and then returned to the furnace. Heating and cooling was repeated until the front side of the

Table 1
Mass fractions of raw materials used in sample preparation.

Components	Mass (%)
Chamotte	40
Bauxite	40
Clay	20

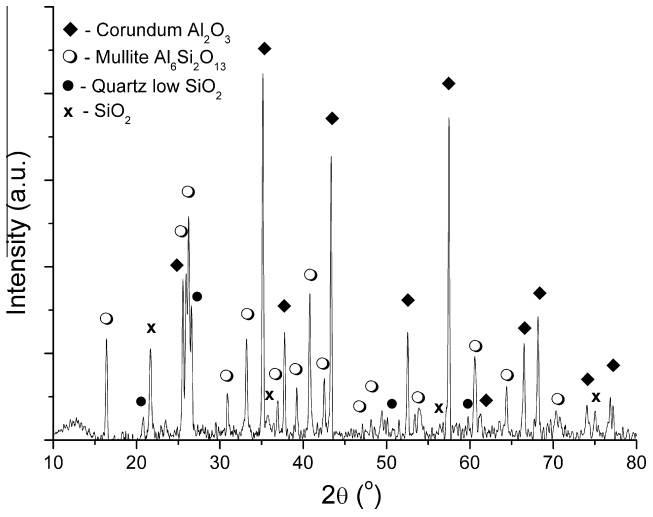

Fig. 1. Mineralogical composition of the sintered sample. The identified phases in the specimen were: corundum, quartz, silicon oxide and mullite.

sample exhibited 50% surface damage. The number of quenches to failure was taken as a measure of thermal shock resistance. In this study image analysis was used for the determination of surface damage level before and after defined numbers of quenches, and to determine the characteristic defect shape of the two materials prepared using different pressures.

3. Finite element modeling

The temperature and stress/strain in the specimens produced at a pressure of 50 MPa were determined by finite element analysis, using the software package Abaqus [21]. Three-dimensional FE models were considered, using symmetry whenever possible. One of the models is shown in Fig. 2a; it is 1/8 of the disk (sample) with or without an idealized defect. Mechanical and thermal boundary conditions (symmetry and convection, respectively) are shown in Fig. 2b.

The modeling was based on the assumption that all defects are due to thermal shock, and caused by thermal stresses. The stress contours were given for several idealized geometries of the defects. The reasoning behind this was following: the surface area and depth of the majority of the analyzed defects were set as equal to the average experimentally determined values. Three main shapes were chosen: ellipsoidal (without sharp corners), pyramid-shaped (with sharp edges and a pronounced tip) and irregular (several pyramids). These defects simulated the actual defects caused by the thermal shock and observed at the surface (taking into account the average dimensions), and the aim was to determine the influence of defect geometry on the stress state. Experimental tests revealed presence of defects, but no defects with significantly larger depth than 1 mm were observed on the surface of the specimens.

The modeling of the analyzed problem required the use of finite elements with both temperature and displacement degrees of freedom. Abaqus/Standard transient analysis was conducted, and tetrahedral elements C3D4T were used – 4-node thermally coupled tetrahedral, linear displacement and temperature. The mesh is refined in the vicinity of the defect, to capture the stress gradients more accurately.

The refractory materials were subjected to sudden temperature changes (thermal shock), which induced transient stress/strain field in the material. Calculation of these fields required the use of material properties given in Table 2. Thermal properties were taken from the producer's specification, while mechanical properties were measured by authors on the sintered samples [23].

Table 2
Properties of the alumina based material used in finite element analysis [26].

Thermal properties	
Thermal conductivity, λ (W/mk)	1.32
Specific heat, C_p (kJ/kg K)	1.05
Thermal expansion coefficient, α (%)	0.7
Physical and mechanical properties	
Density, ρ (g/cm^3)	2.05
Compressive strength, σ_p (MPa)	35
Young's modulus of elasticity, E (MPa)	9.88
Poisson ratio, ν	0.2

As for the heat transfer coefficient, which was used for the convective heat transfer, it was considered as variable due to the very sudden temperature decrease. In authors' previous work [24,25], different heat transfer conditions were considered and the extreme values (for the highest and lowest temperature during the cooling) were used in this analysis. The heat transfer was characterized through a linear dependence on temperature, with the value 300 W/m^2 K at room temperature and 3000 W/m^2 K at 950 °C (which was the heating temperature for the samples and hence the initial condition for the calculation).

4. Results and discussion

Two specimens having different preparation conditions were considered for the experimental study of the shape of the defects that occurred during thermal shock. Specimens pressed under 36 MPa and 50 MPa were examined. Typical forms of the surface defects are presented in Fig. 3a and b, from which it is obvious that the two specimens differed in the total amount of surface destruction as well as the form of the defects. The specimen pressed at 50 MPa had less total surface destruction but larger individual defects. Table 3 shows that the morphological characteristics of the defects differed.

In Fig. 4, the measured surface degradation after every four thermal shock cycles was presented. Surface degradation was measured using image analysis software (Image ProPlus version 4.0 produced by Media Cybernetics). The samples were colored using the blue chalk so that the part of the sample that had no damage became blue and the part with damage preserved the original color. The procedure was than established to determine the overall damage of the sample as those colors differ and enabled the detection of damaged zones on the specimen's surface.

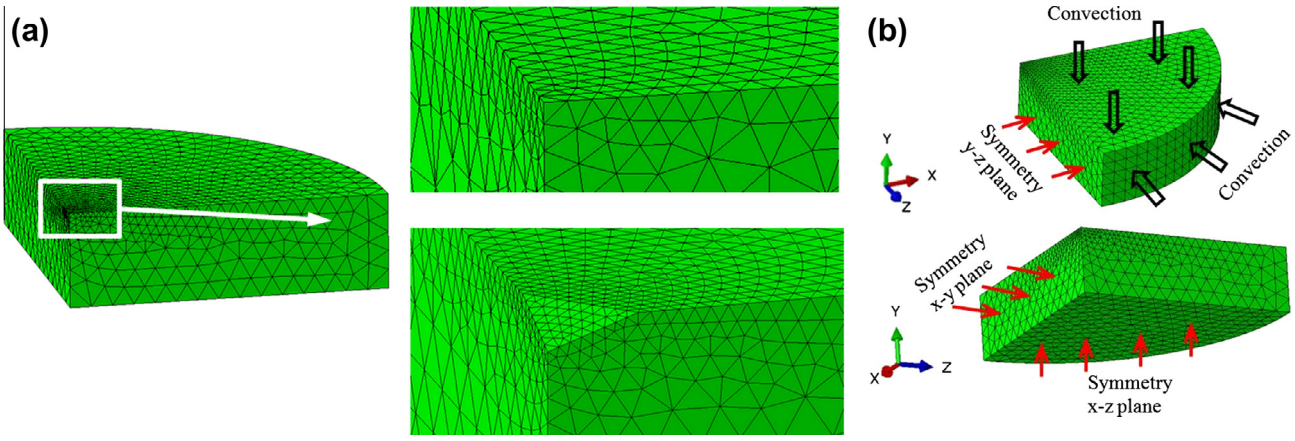

Fig. 2. (a) The finite element (FE) mesh of a specimen with one single symmetrically placed defect and with no defects at all, and (b) mechanical and thermal boundary conditions (symmetry and convection).

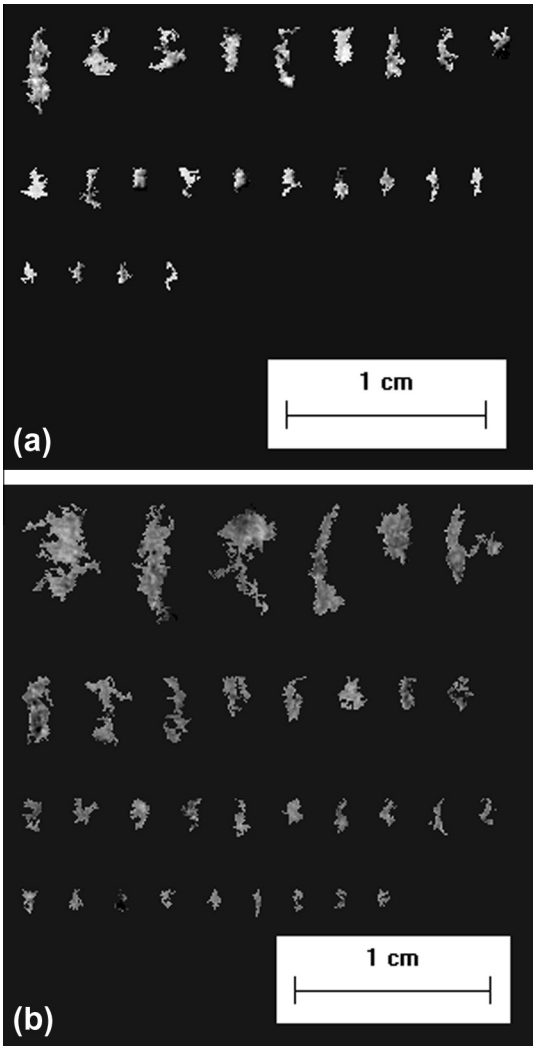

Fig. 3. Typical defects on the surface of thermally shocked specimens pressed at (a) 36 MPa and (b) 50 MPa.

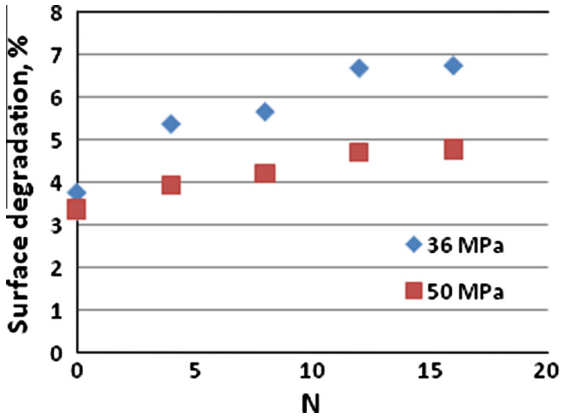

Fig. 4. Level of surface damage *P*/*Po* in relation to the number of cooling cycles *N* and the specimen preparation conditions.

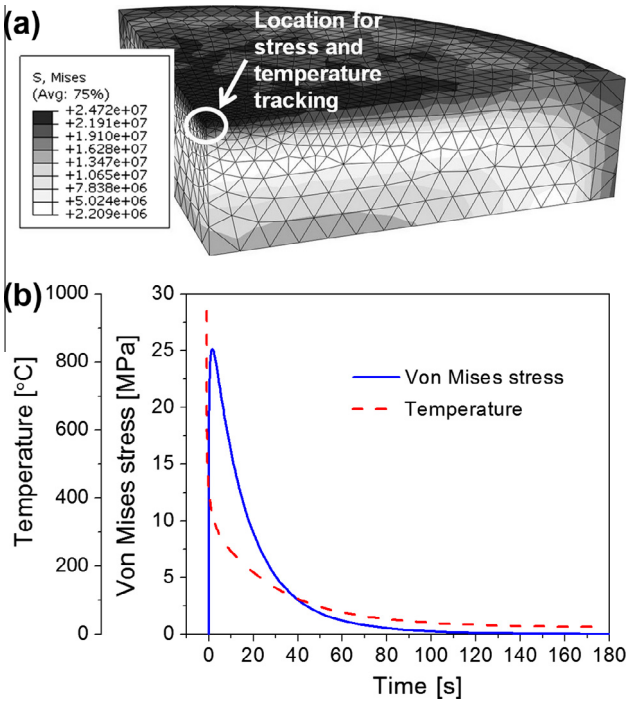

Fig. 5. Equivalent von Mises stress for the sample without damage.

Image analysis of surface degradation was used to separate destructed and nondestructed part of the specimen surface. Ratio of increase of surface damage to the original surface was chosen as the parameter for surface damage characterization, as in previous authors' papers [27–30]. Previous work included correlation of the surface destruction to the material resistance factors and to the changes of material properties. This showed that the destruction level was proportional to the degradation of thermo-mechanical properties of materials [31–33]. The assessment of stress field that develops in the interior of the specimen after each quench test was the point of this study. Special interest was to calculate the influence of the shape and size of surface defect on the stress field

Table 3
Characteristical statistical parameters of the defects observed on specimens pressed at 36 MPa and 50 MPa.

	36 MPa			50 MPa		
	Area	Diameter (mean)	Fractal dimension	Area	Diameter (mean)	Fractal dimension
Mean (mm)	1.395	1.269	1.284	0.8145	1.061	1.238
Standard error	0.2727	0.129	0.0146	0.1094	0.0941	0.01293
Median (mm)	0.6798	0.9506	1.279	0.6334	0.9371	1.2439
Standard deviation	1.567	0.7420	0.0836	0.5249	0.4514	0.0620
Sample variance	2.454	0.5506	0.0069	0.2755	0.2037	0.0038
Range	5.678	2.6229	0.3431	2.263	1.999	0.2282
Minimum (mm)	0.2394	0.4714	1.121	0.2935	0.4793	1.133
Maximum (mm)	5.917	3.094	1.464	2.557	2.479	1.361
Sum	46.03	41.89	42.38	18.73	24.41	28.48

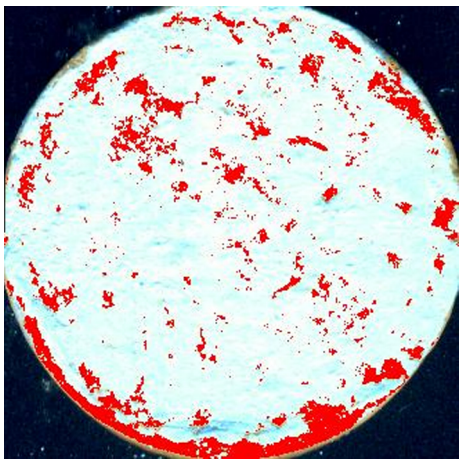

Fig. 6. A sample with damage occurring during thermal shock.

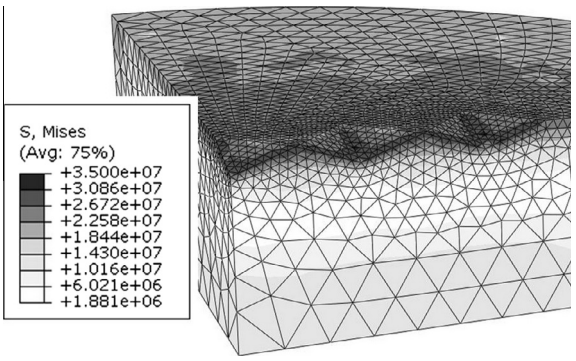

Fig. 8. Equivalent von Mises stress for a sample in the form of three grooves with a depth of 0.5 mm.

developed on the material. This was accomplished by using the finite element method in order to determine the residual stresses and to prove that the defects mostly tend to grow on surface, rather than increasing their depth.

As mentioned in the previous section, models for samples without damage and models with different shapes and sizes of damage were made. The material having no damage was used as reference to compare the influence of damage shape and size on the stress field obtained in the specimen. Equivalent von Misses stress for the model without damage was shown in Fig. 5.

The dependence of von Mises stress and temperature on time (given in Fig. 5b) was obtained in the middle of the upper surface of the specimen (location is marked in Fig. 5a). The explanation for very sudden stress decrease could be found in the testing conditions, because the specimen was not constrained in any direction during the cooling.

The value obtained by the finite element analysis in the middle of the upper surface of the specimen (Fig. 5a) was 24.72 MPa. It was smaller in comparison with the ultimate strength of the

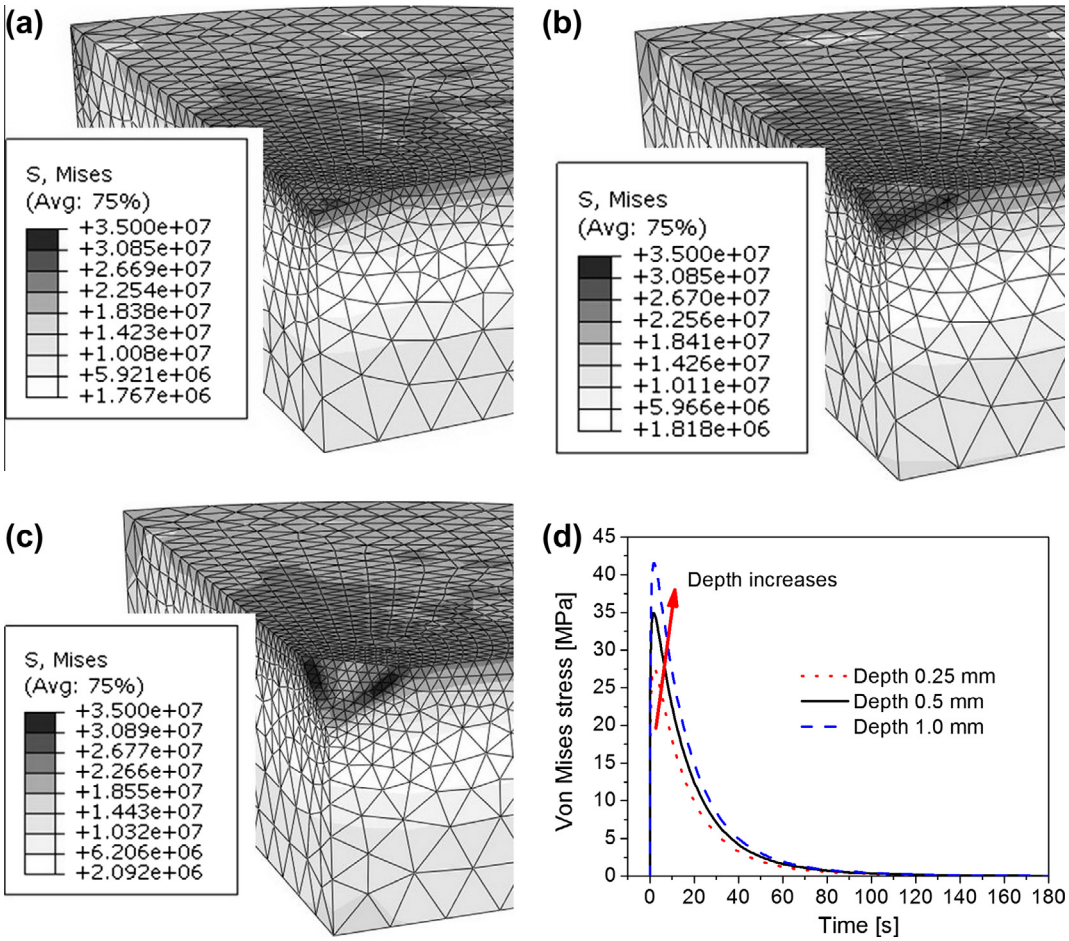

Fig. 7. Equivalent von Mises stress for the sample in the form of grooves with different depth of damages: (a) 0.25 mm, (b) 0.5 mm, (c) 1 mm, and (d) change of the stress value with time.

material (approx. 35 MPa), but the presence of local heterogeneities or pores could cause stress concentration on the local level, which could lead to damage initiation. This value was achieved approximately 3 s after immersing in water and after this peak the stress values decreased. The stress was the largest on the edge and in the middle of the sample, where the damage actually occurred, Fig. 6.

The dimensions of the damages were approximated from the experimental data. The damaged surface of the sample was analyzed in the program *Image Pro Plus*. The obtained data revealed that the average diameter of damage was about 2 mm and the damage taken for the calculations was approximated to 2 mm.

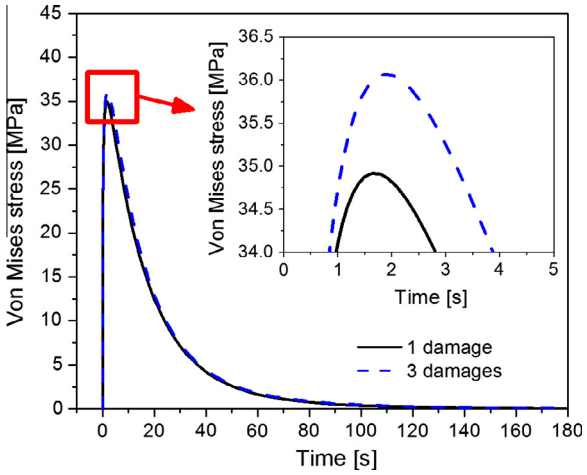

Fig. 9. Change of the equivalent von Mises stress with time for 1 and 3 damages.

The damages were presented in the form of grooves with three different depths (0.25, 0.5 and 1 mm) and in the form of an ellipsoid with a depth of 0.5 mm. The goal of this research was to analyze the influence of the width and depth of the damage on the inducted stress. The results of the equivalent von Mises stress for all models are shown in Fig. 7.

The obtained results showed that the stress increased with increasing depth of damage. The stress level remained the same when the length of the damage increased (when there were several damages in series), Figs. 8 and 9.

In the case of damage of depth 1 mm, the stress concentration does not appear at the bottom, but closer to the surface. The fact that the stress concentration (for a depth of 1 mm) is closer to the surface than to the bottom may explain why only a small number of defects were deeper than 0.5 mm and that the surface damage grew but generally did not exceed a depth of 0.5–1 mm. The model with ellipsoid-shaped damage had a slightly less pronounced stress concentration compared with the same shape groove depth.

Besides the regularly shaped defects, considered in the previous part of the text, random-shaped damages were also modeled in accordance with the shapes observed on the actual specimens. The surface and depth of these defects (analyzed as several randomly positioned pyramids near the middle of the disk) were similar to the surface and depth of single defects shown in Fig. 10. Of course, symmetry conditions were not applied in this case, due to the irregular geometry of the defects.

Equivalent von Mises stress field for an irregular defect shape is shown in Fig. 11. Very high values were obtained in the ligaments between the defects, which mean that the ligaments tend to fail first, causing the single defects to join.

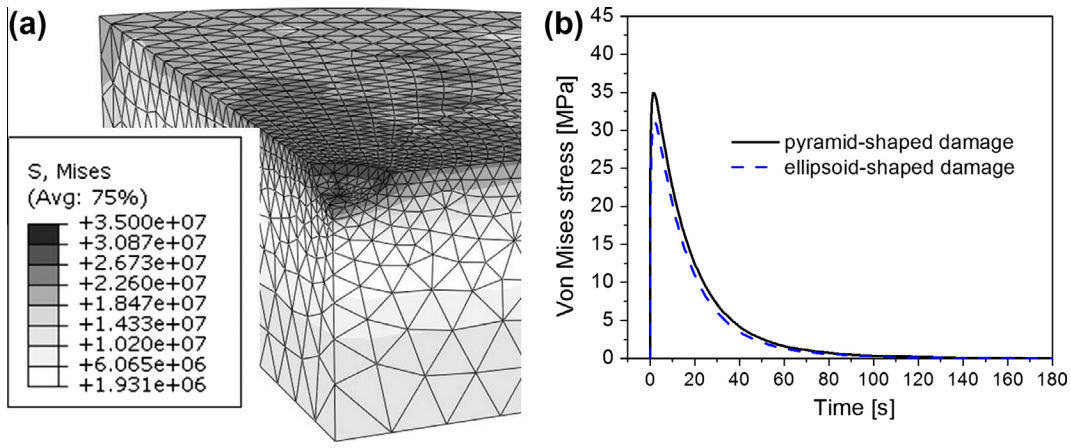

Fig. 10. Equivalent von Mises stress for a sample in the form of an ellipsoid with a depth of 0.5 mm (a) and changes in the stress value with time for pyramid-shaped and ellipsoid-shaped damages (b).

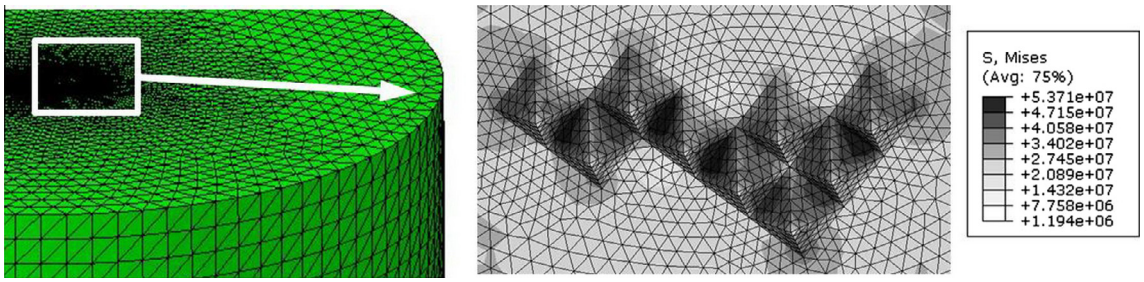

Fig. 11. Equivalent von Mises stress for a sample with a randomly distributed damage shape.

It can be said that differences between the results obtained for different damage geometries were both qualitative and quantitative – it was determined that stress concentration for larger defect depths (surface area was the same and corresponding to the average experimental one) favored the increase of surface area, rather than depth increase. Hence, the stress state could explain the absence of defects with larger depths on the surface of the specimens. Similar behavior was experimentally observed on different refractory material, silicon carbide/cordierite composite [10]. This is also in agreement with the findings of Yuan et al. [6], who reported pronounced lateral crack growth in alumina exposed to thermal shock. On the other hand, the analysis of a randomly formed damage (several pyramids forming an irregular shape) that mostly looked like the realistic ones, showed that the smaller defects would tend to merge into a single larger one.

5. Conclusions

Alumina-based ceramic material exposed to thermal shock was considered in this paper. Calculation of temperature and stress distribution enables a visualization of the stress field and especially the stress concentration. When compared to an image of a specimen previously subjected to thermal shock, it was obvious that the main surface destruction was obtained in the regions of the maximum stress level. Different specimen preparation routes resulted in different shapes of the surface defects that have some morphological characteristics which enabled the observation of the influence shape and size on further stress concentration.

The analysis of simplified damages (shaped like one or more pyramids or ellipsoids) showed that the stress level obtained using FEM depended on the shape of the defect, while it was not significantly affected by the length (in case of several joined defects). The depth of the defect also influenced the stress level. It was registered that in the case of 1 mm damage depth, the stress concentration was not at the bottom of the damage but near the specimen surface, which favored an increase in damaged area rather than the depth of the damage. The models with irregular damage shape (composed of several irregularly distributed pyramids) were characterized by very high stress levels in the ligament between the single defects, which means that the ligaments tend to fail first, causing the joining of single defects.

For all finite element models, the maximum stress levels were obtained during the first few seconds of cooling, while after 180 s of cooling, the stress values decreased to almost zero, resulting in practically no residual stresses in the material.

The practical significance of the present work could be seen into two directions. The first is the simulation of the conditions required for the water quench test and analyzing the induced thermal stresses and their influence on defect formation and growth of crack and their influence on the mechanical behavior during the test. Other approach would be to employ this model and the obtained result to preparation conditions different to those of the standard procedure (for example different temperature range, temperature lower and higher than 950 °C).

Main scientific significance of this work was to study how different surface defects developed and what were the most probable ways of their development. From the studies presented in this paper, it is clear that even the mean value of the diameters of the defects were different for specimens prepared using different compaction pressures. The defect presenting the real shape of the surface destruction was the typical one found on the surface of one of the studied specimens. The geometry was simplified and the aim of the study was to clarify the manner in which thermal shock influences such a defect, and to establish some criteria that could be guidance for producers of refractory materials to alleviate the most dangerous features of defects occurring at the surface.

Acknowledgements

This research has been financed by the Ministry of Education, Science and Technological Development of the Republic of Serbia as a part of the Projects TR34011 and III45012. B.M. and M.R. acknowledge the support of the Ministry of Education, Science and Technological Development of the Republic of Serbia through the Project ON174004.

References

[1] Lee KS, Jang KS, Park JH, Kim TW, Han S, Woo SK. Designing the fiber volume ratio in SiC fiber-reinforced SiC ceramic composites under Hertzian stress. Mater Des 2011;32:4394-01.
[2] Coppack TJ. A method for thermal cycling refractories and an appraisal of its effects by a non-destructive technique. Trans J Br Ceram Soc 1981;80:43–6.
[3] Kingery WD. Factors affecting thermal stress resistance of ceramic materials. J Am Ceram Soc 1955;38:3–15.
[4] Hasselman DPH. Strength behavior of polycrystalline alumina subjected to thermal shock. J Am Ceram Soc 1970;53:490–5.
[5] Hasselman DPH. Unified theory of thermal shock fracture initiation crack propagation in brittle ceramics. J Am Ceram Soc 1969;52:600–4.
[6] Yuan C, Vandeperre LJ, Stearn RJ, Clegg WJ. The effect of porosity in thermal shock. J Mater Sci 2008;43:4099–106.
[7] You XQ, Si TZ, Liua N, Rena PP, Xua YD, Feng JP. Effect of grain size on thermal shock resistance of Al_2O_3–TiC ceramics. Ceram Int 2005;31:33–8.
[8] Tacibana F, Enya S. Heat transfer problems in quenching. Bull JSME 1973;16:100–9.
[9] Volkov-Husović T, Jančić-Heinemann R. Thermal stability of refractories: testing, analysis, modeling. Association of Metallurgical Engineers, in Serbian, Belgrade; 2005.
[10] Dimitrijević MM, Pošarac M, Majstorović J, Volkov-Husović T, Matović B. Behavior of silicon carbide/cordierite composite material after cyclic thermal shock. Ceram Int 2009;35:1077–81.
[11] Murugan N, Narayanan R. Finite element simulation of residual stresses and their measurement by contour method. Mater Des 2009;30:2067–71.
[12] Wei S, Qunbo F, Fu-chi W, Zhuang M. Modeling of micro-crack growth during thermal shock based on microstructural images of thermal barrier coatings. Comput Mater Sci 2009;46:600–2.
[13] Li D, Li W, Zhang W, Fang D. Thermal shock resistance of ultra-high temperature ceramics including the effects of thermal environment and external constraints. Mater Des 2012;37:211–4.
[14] Liu H, Tao J, Gautreau Y, Zhang P, Xu J. Simulation of thermal stresses in SiC–Al_2O_3 composite tritium penetration barrier by finite-element analysis. Mater Des 2009;30:2785-0.
[15] Celik E, Islamoglu Y, Akin Y, Hascicek YS. Thermal analysis of high temperature ZrO_2 insulation ceramic coatings on Ag tapes used as sheath of Bi-2212 superconducting materials using finite element method. Mater Des 2003;24:543–6.
[16] Dube M, Doquet V, Constantinescu A, George D, Remond Y, Ahzi S. Modeling of thermal shock-induced damage in a borosilicate glass. Mech Mater 2010;42:863–72.
[17] Tomba AG, Cavalieri AL. Numerical simulation of the thermal shock of alumina disks with different surface finish. J Eur Ceram Soc 2001;21:1205–12.
[18] Hvizdoš P, Jonsson D, Anglada M, Anné G, Van Der Biest O. Mechanical properties and thermal shock behaviour of an alumina/zirconia functionally graded material prepared by electrophoretic deposition. J Eur Ceram Soc 2007;27:1365–71.
[19] Nakonieczny K, Sadowski T. Modelling of 'thermal shocks' in composite materials using a mesh free FEM. Comput Mater Sci 2009;44:1307–11.
[20] Saâdaoui M, Fantozzi G. Crack growth resistance under thermal shock loading of alumina. Mater Sci Eng A 1998;247:142–51.
[21] Abaqus Analysis User's Manual, Simulia; 2012.
[22] Standard: SRPS B.D8.319. Refractories – methods of physical testing – determination of the resistance to thermal shock – water quenching. Institute for Standardization of Serbia; 1987 [in Serbian].
[23] Dimitrijević MM, Veljović Dj, Posarac-Marković M, Jančić-Heinemann R, Volkov-Husović T, Zrilić M. Mechanical properties correlation to processing parameters for advanced alumina based refractories. Sci Sinter 2012;44:25–33.
[24] Volkov-Husović T, Jančić RM, Popović ZV, Raić KT. Selection of the method of calculation temperature distribution in refractory specimen (99% Al_2O_3). Interceramics 1998;47:230–5.
[25] Volkov-Husović T, Jančić RM. Influence of natural convection on thermal stability of refractory specimen. Metalurgija-J Metall 2001;7:59–67.
[26] [Internet]. BOMEX Holding. c2010- [cited 2012 Dec 1]. <http://www.bomexholding.com/>.

[27] Volkov-Husović T, Jančić RM, Mitraković D. Using the image analysis program for prediction of thermal stability behavior of refractory specimen. Mater Sci Forum Funct Graded Mater VIII 2005;492–493:561–5.
[28] Posarac M, Dimitrijevic M, Volkov-Husovic T, Devecerski A, Matovic B. Determination of thermal shock resistance of silicon carbide/cordierite composite material using nondestructive test methods. J Eur Ceram Soc 2008;28:1275–8.
[29] Martinovic S, Dojcinovic M, Dimitrijevic M, Devecerski A, Matovic B, Volkov-Husovic T. Implementation of image analysis on thermal shock and cavitation resistance testing of refractory concrete. J Eur Ceram Soc 2008;30:3303–9.
[30] Boccaccini DN, Kamseu E, Volkov-Husovic TD, Cannio M, Romagnoli M, Veronesi P, et al. Characterization of thermal shock damage in cordieritemullite refractory material by non-destructive methods. In: Fourth Balkan conference on metallurgy, Zlatibor, proceedings; 2006. p. 503–9.
[31] Dimitrijevic MM, Jancic Heinemann R, Volkov Husovic T, Posarac M, Majstorovic J. Morphological analysis of surface degradation of advanced alumina based refactories subjected to thermal shock. In: Proc engin, vol. 10; 2011. p. 2153–7.
[32] Volkov-Husovic T, Jancic RM, Cvetkovic M, Mitrakovic D, Popovic Z. Thermal shock behavior of alumina based refractories: fracture resistance parameters and water quench test. Mater Lett 1999;38:372–8.
[33] Volkov-Husovic T, Jancic Heinemann R. Thermal shock behavior of alumina based refractories: comparison with the mechanical data and thermal stability behavior prediction. Silic Ind 2008;73:201–5.